Effect of mono- vs. bi-functionality of aminophosphonate derivatives on the enhancement of U(VI) sorption: physicochemical properties and sorption performance

Enas Imam, Ahmed Hashem, Ahmad Tolba, Mohammad Mahfouz, Ibrahim El-Tantawy El-Sayed, Ahmed El-Tantawy, Ahmed Galhoum, Eric Guibal

Effect of mono- vs. bi-functionality of aminophosphonate derivatives on the enhancement of U(VI) sorption: physicochemical properties and sorption performance

Enas A. Imam [a,*], Ahmed I. Hashem [b], Ahmad A. Tolba [a], Mohammad G. Mahfouz [a], Ibrahim El-Tantawy El-Sayed [c], Ahmed I. El-Tantawy [c], Ahmed A. Galhoum [a,*], Eric Guibal [d]

[a] Nuclear Materials Authority, P.O. Box 530, El-Maadi, Cairo, Egypt
[b] Chemistry Department, Faculty of Science, Ain Shams University, Cairo, Abassia, Egypt
[c] Chemistry Department, Faculty of Science, Menoufia University, Shebin El-Kom, Egypt
[d] Institut Mines Telecom – Mines Alès, Polymer Composites and Hybrids, 6 avenue de Clavières, F-30319 Alès cedex, France

A B S T R A C T

Aminophosphonates are excellent complexing agents for numerous metal ions (including uranyl). Based on this property, two sorbents have been synthesized using simple one-pot reaction: thiocarbazide (amine source), p- phthaldehyde (di-aldehyde), and trimethylphosphite (phosphorous precursor) are mixed with different molar ratios to produce bis- (2:1:2) and mono (1:1:1) α-aminophosphonate-based derivatives (B-AmPh and M-AmPh, respectively). Materials are characterized using XRD, BET, SEM, titration, elemental, FTIR, and XPS analyses to evaluate the effect of substitution rate on the physicochemical properties. FTIR and XPS are also used for elucidating binding mechanisms. Sorption properties of the materials have been tested for U(VI): the pH effect is completed by investigating uptake kinetics and sorption isotherms. At pH 4.5 (and T: 55 °C), sorption capacity increases from 0.89 to 1.22 mmol/g with the increase in the substitution degree (M-AmPh < B-AmPh). This increase is not correlated to the fraction of grafted reactive groups, meaning that steric hindrance probably contributes to limiting the accessibility and availability of aminophosphonate moieties. Pseudo-second order and Crank equation preferentially fit kinetic profiles. Langmuir equation successfully describes sorption isotherms. Sorption process is systematically endothermic and spontaneous: enthalpy and entropy changes decrease with the substitution rate. Uranium successfully desorbed using HCl (0.2 M); allows six cycles of re-use with limited loss in sorption/desorption efficiencies. The sorbents were used for U(VI) recovery from acidic leachate of uranium ore. This test shows remarkable affinity and selectivity of B-AmPh for uranium; however, after elution and precipitation the U concentrate contains about 10 % of impurities.

Keywords:
Uranyl recovery
Aminophosphonate functionality
Reactive group intensity
Sorption studies
Uranium ore leachate

1. Introduction

Uranium is both an extremely valuable source of energy and a major pollutant in radioactive wastewater. The half-life of uranium (issued from fission by-products) explains the long-term residual radioactivity of wastewater [1–3]. Several causes may explain its presence in groundwater systems, such as natural and anthropogenic leaching from mining tailings, phosphate fertilizer dissolution, nuclear reactors, and coal-fired power plants. The inherent toxicity, existence, and accumulation in the food chain may explain that environmental laws are becoming increasingly stringent concerning uranium discharge. For these reasons, uranium separation and recovery from contaminated water are strategic issues both for effective uranium resource usage (especially low-grade mineralization) and environmental preservation [3–6]. Precipitation, solvent extraction, and impregnated resins can all be used to remove metal ions from aqueous solutions; however, sorption techniques are more suited to diluted effluents due to the fast kinetics, ecofriendly, good selectivity, high efficacy and reusability. The most commonly investigated sorbents for uranium recovery in sorption processes are impregnated resins [7], chelating or ion-exchange resins [6, 8–10]. Biopolymers (i.e., cellulose, chitosan) [4,6,11], inorganic sorbents (i.e., metal oxides, metal–organic frameworks, clay minerals,

* Corresponding authors.
E-mail addresses: enasimam420@yahoo.com (E.A. Imam), Galhoum_nma@yahoo.com (A.A. Galhoum).

mesoporous silica) [3,12,13], and carbon-based materials (i.e., activated carbon, graphene oxides) [5,6].

Chelating resins are polymers bearing specific reactive groups that chelate metal ions according to Pearson theory (HSAB, [14]) considering that uranium is a hard acid that prefers to attach to hard bases [2,4]. Chelating resins that contain reactive groups such as N, P, O and S are highly efficient ligands for selective uranium sorption with high capacity [5,6,13,14]. Organophosphorus compounds have received a considerable attention in the last decade as a result to their agricultural, pharmacological, biological, and medicinal properties; also they are used as synthetic intermediates [15]. These organophosphorus compounds and their derivatives are also used as industrial chemicals in water treatment, metal extraction, and pollution management and as excellent metal-complexing agents for different transition metals with diagnostic and therapeutic uses [13,16,17]. Organophosphorus compounds e.g. minophosphonates have just a wide range of applications as α-aminophosphonates are structurally similar to α-amino acids in which the carboxylic moiety is substituted with a phosphonic acid or analogous group [16]. They are also employed as ligands in organocatalysis and transition-metal catalysis [18,19]. However, novel materials with specific functions, excellent extraction properties, and high stability based on this type of chemical structure are still needed. It is also necessary to implement the knowledge of how the substituents grafted on the ligand may improve or reduce sorption efficacy. The study of uranium extraction using tributyl phosphate (TBP) and trialkylphosphine oxides (TRPO) revealed that the P = O group (of these extractants) had a significant coordination effect with uranyl ions [20]. In addition, stable bioactive phosphate analogues are commonly produced depending on the hydrolytic stability of C-P bonds in the α-aminophosphonate group [21]. Recently, it has been suggested that using multi-functional groups on resins, such as amino, carboxymethyl, phosphonate, or thiocarbonyl groups, is a promising technique for developing highly metal selective sorbents with improved sorption performance and high reactivity [22–25]. The Alexandratos Group reported the effect bi-functionality on metal selectivity and sorption criteria, in association with acid and base characteristics, hydrophilic effect, and intra-ligand collaboration [26,27]. The multifunctional materials have the advantageous of a) improved sorption capacities due to the increased reactive groups content, b) the selectivity resulting from the interaction of vicinal functions, and c) the optimal pH range for maximum sorption [4,24]. Some aminophosphonate compounds have already been produced and evaluated for uranium binding [2,4,6,11,28], rare earth [29], heavy metals [17]. The chemical environment through the effects of induction, steric hindrance, acid-base properties, or dual functionalities may significantly affect the reactivity of phosphonate groups in multifunctional sorbents. Varying the molar ratios of the reactants during the synthesis may also affect the global sorption properties of the resins because of modulations in the number (or density) of reactive groups, also their molecular arrangement in the final product.

Till now, the scope of our study with the concerned subjects has not been reported in any published work in the literature. Herein, a simple one-pot synthesis reaction was used to prepare two new α-aminophosphonate derivatives; via the reaction between thiocarbazide, trimethylphosphite, and p-phthaldehyde with different amounts of thiocarbazide and trimethylphosphite. The physicochemical structure and chemical properties of the materials were initially determined by FTIR (Fourier transform infrared spectroscopy), XPS (X-ray photoelectron spectroscopy), XRD (The X-ray diffraction), BET (the Brunauer–Emmett–Teller method), elemental analysis (CHN/O) and pH at point of zero charge (pH_{PZC}). In a second step, the uranyl sorption properties were compared for the two sorbents through the study of sorption parameters including pH, uptake kinetics, sorption isotherms with thermodynamics. Finally, the regeneration and reusability of the two materials was evaluated before testing their application on mining effluent for uranium recovery. The comparison of physicochemical properties and sorption performances will be discussed in relation with the grafting of mono- and bi-aminophosphonates (M-AmPh and B-AmPh). This work is part of a general research where the impact of the environment of reactive groups (substitutes on aminophosphonate) is investigated to optimize sorption performances. The specific objective here consists of evaluating the impact of the density of reactive groups (controlled by molar ratios) on sorption performances: based on the mass balance considering the amounts of reagents used for the synthesis of the sorbents, compared with the complete reaction, the yields of the synthesis were 88.9 % and 84.8 % for M-AmPh and B-AmPh, respectively.

2. Materials and methods

2.1. Synthesis of materials

The detailed information for all used chemicals and materials was displayed in (Section A, SI). The synthesis route for the two sorbents and their proposed structures are shown in Scheme 1. Thiocarbazide (as amine source), p-phthaldehyde (di-aldehyde), and trimethylphosphite with different molar ratio (2:1:2) and (1:1:1) (for preparing B-AmPh and M-AmPh, respectively) were dissolved in CH_3CN (5 mL) and washed-up with ethanol. The mixture was allowed to stir for 15 min at room temperature followed by instantly adding the Lewis acid catalyst (Copper(II) triflate, 20 % of the entire mixture by weight). The mixture was left to stir for 3 days at room temperature [4]. The final products were filtered and washed with acetonitrile before being left to air-drying. Finally, the dry powders were placed in a desiccator for later use. The obtained materials were deeply characterized and more detailed information for the different characterization techniques was displayed in (Section A, SI).

2.2. Metal sorption-desorption experiments

Sorption tests were performed in batch systems. A fixed volume (V, 50 mL) of solution (initial concentration C_0, 0.21 mmol/L, at given initial pH value, pH_0) was mixed with a specified amount of sorbent (m, 0.025 g). Sorbent dose (SD=m/V) corresponds to 0.5 g/L. Agitation speed was set to 200 rpm, while standard temperature was 25 ± 1 °C. At fixed contact times (for uptake kinetics) or at equilibrium, samples were collected, filtrated with membrane filter and analyzed for determination of residual concentration (C(t) or C_{eq}, mmol/L). The final pH was also systematically recorded. Uranium concentration was monitored using the so-called Arsenazo III colorimetric method [30]. Absorbance was measured at 655 nm wavelength using a SP-8001 Metertech spectrophotometer (Metertech Inc., model SP-8001, Taipei, Taiwan). The mass balance equation ($q_e=(C_0-C_{eq})\times V_{(L)}/m_{(g)}$) was used to calculate the sorption capacity, while the distribution ratio corresponds to D (L/g): q_{eq}/C_{eq}. For sorption isotherms, the initial concentration was varied in the range 0.12–1.28 mmol/L (pH_0 being fixed to 4.5, shaking at 200 rpm for 1 h, and SD at 0.5 g/L). The obtained sorption results were fitted using conventional kinetics and isotherms models (Tables S1a and b) and thoroughly discussed in (Section B, SI). For metal desorption and sorbent recycling, 0.2 M HCl solution was used as the eluent; a 1-hour contact time was sufficient for achieving the desorption of the metal. The sorption capacity at the sixth cycle was compared to the value reached at the first step. The mass balance equation was also used for quantifying the desorption efficiency. Experiments are systematically duplicated and the figures show the average values (with standard deviations). The treatment of precipitated pregnant leaching solution (PPLS, Section E, SI) was operated in batch reactor under experimental conditions comparable to those used for synthetic solutions (pH_0: 4.5; SD: 0.5 g/L; time: 60 min; room temperature (25 ± 1 °C); and agitation speed: 200 rpm).

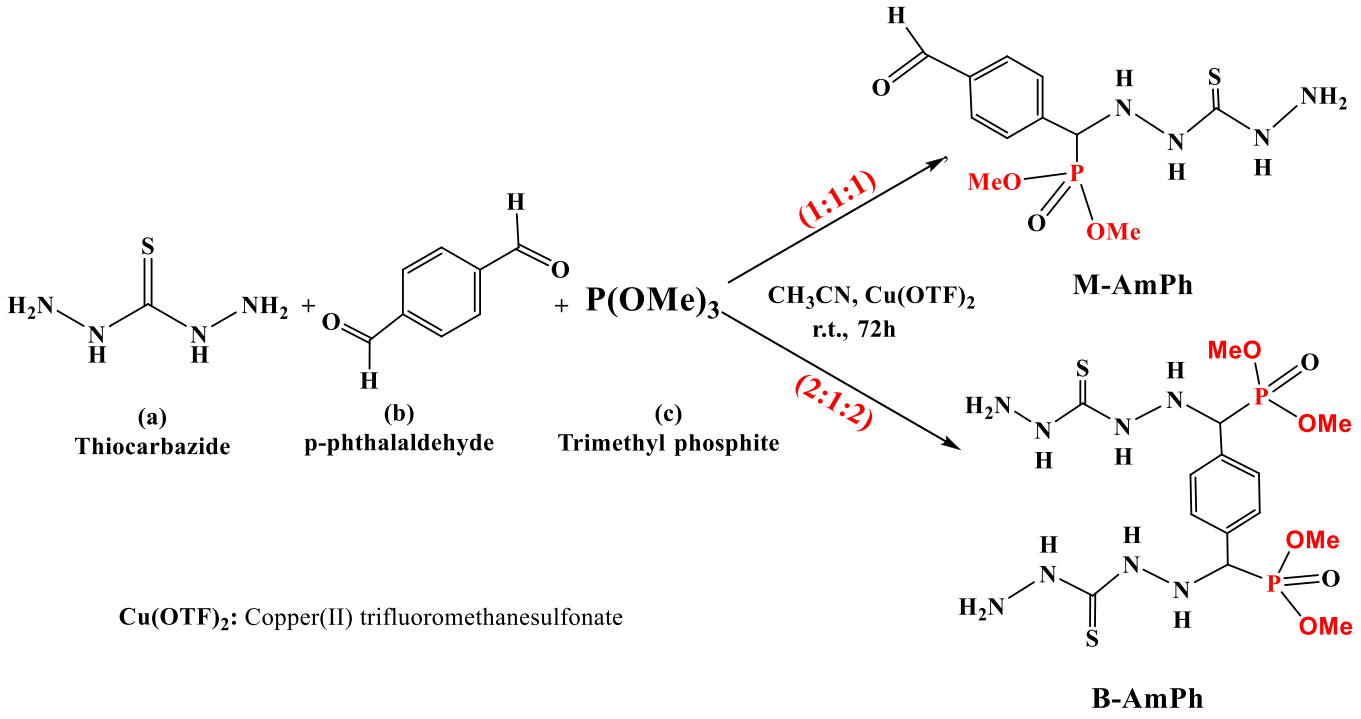

Scheme 1. The synthesis route of α-aminophosphonate sorbents (B-AmPh and M-AmPh).

3. Results and discussion

3.1. Sorbent synthesis

Schematic reaction pathway for grafting methylphosphite on thiocarbazide-based support for the synthesis of aminophosphonate sorbents was illustrated in Scheme S1. More detailed information for the synthesis mechanism and its different stages were extensively discussed in (Section C, SI).

3.2. Characterization

3.2.1. Morphological observations–SEM

The SEM observation of sorbent particles shows a majority of rounded and irregular particles (Table S2). The distribution of particle size (histogram plots) was obtained by image analysis (these data were acquired using the Foxit Phantom PDF properties for estimating tool distances and Origin 2018 for creating histograms) performed on 210 and 158 particles for B-AmPh and M-AmPh, respectively. B-AmPh is characterized by an average particle size close to 11.2 ± 5.7 μm; little smaller than M-AmPh at 16.2 ± 8.6 μm (wider size dispersion).

3.2.2. SEM-EDX analysis

EDX associated to SEM observations allows semi-quantitatively analyzing the surface of the sorbents before and after U(VI) sorption (Table S3). The phosphonomethylation reaction is confirmed by the appearance of the signal at 2.01 keV corresponding to K_α P signal and a weak peak at 0.392 keV for K_α N signal (poor sensibility). A large peak appeared around 2.3 keV corresponding to K_α S. The signals specified at energies of 0.525 keV and 0.277 keV correspond to O $k_\alpha 1$ and C k_α peaks respectively [31]. The N content of B-AmPh sorbent is somewhat larger than that of M-AmPh sorbent, which is compatible with elemental analysis theoretical values (see below). After U(VI) sorption, EDX investigation of the sorbents obviously demonstrates the appearance of a U signal characterized by the peaks of U (at ~3.2 and 13.8 keV) supported by a higher intensity for the S-element: this may be attributed to sorption of U as sulfate species or direct sulfate binding (or both). The U mass fractions of the two sorbents were 18.26 % and 15.41 % (w/w) for B-AmPh and M-AmPh, respectively. After metal sorption, it is noted that N element intensity decreases; likely due to examination effect (poor sensitivity) or its contribution in adsorption reaction (masked signal). The existence of trace elements (such as Si, Ca, Al and Fe) may result from material contamination during the preparation of samples SEM-EDX analysis.

3.2.3. Elemental analysis

Elemental analyses of B-AmPh and M-AmPh sorbents are reported in Table S4. The determination of P element demonstrates the successful phosphorylation; the P content reaches up to 11.51 % and 9.32 % (i.e., 3.72 and 3.01 mmol/g) for B-AmPh and M-AmPh, respectively. Chemical structures were drawn using ChemDraw Professional 15.0. Table S4 lists the proposed theoretical chemical formulae of the synthesized sorbents with their corresponding molecular weights and predicted mass percentages for the individual elements. The molecular formulas of the two sorbents correspond to: $C_{14}H_{28}N_8O_6P_2S_2$ (M.F.) for B-AmPh and $C_{11}H_{17}N_4O_4PS$ for M-AmPh. The molecular weight increases from 332.31 g/mol for M-AmPh to 530.5 g/mol for B-AmPh. The extended phosphite grafting onto p-phthaldehyde backbone (in B-AmPh) logically reduces the C mass fraction compared to the value measured in M-AmPh. The C percentage has been reduced from 40.35 % to 32.61 % (i.e., 33.6 and 27.15 mmol/g) in M-AmPh and B-AmPh, respectively (accompanied by a decrease in the mass fraction of O element). The variations in the N and S contents show a reverse trend: the N mass increases from 12.07 to 15.49 mmol/g (whereas S content increases from 3.01 to 3.53 mmol/g) in M-AmPh and B-AmPh respectively. This is consistent with the amounts of reagents used for the synthesis of B-AmPh.

3.2.4. XRD analysis

Fig. S1 (SI) shows the x-ray diffraction patterns of the two sorbents. The two sorbents are globally amorphous; this is confirmed by the poorly resolved patterns. The broad bands identified in the range of 2θ: 13–35 can be attributed to intermolecular and intramolecular hydrogen bonding. Recently, these broad bands were also associated with the

porosity of polymer materials [32,33].

3.2.5. *Textural properties (BET analysis*

N_2 sorption and desorption isotherms are represented in Fig. S2. The BET method was used for the determination of specific surface area S_{BET} of the sorbents. The experimental conditions (and more specifically the ratio between the amine and phosphite precursors and p-phthaldehyde) strongly influence the porous properties. The S_{BET} of M-AmPh reached 95.4 m^2/g, whereas the phosphomethylation of the second aldehyde group considerably reduces the S_{BET} of B-AmPh sorbent to 58.2 m^2/g. The supplementary linkages contribute to limit the specific surface area due to steric hindrance. According to Langmuir classification, the sorption and desorption patterns are classified as Type II isotherms [34]. Narrow hysteresis loops are observed in the isotherms of the two sorbents; this definitely reveals the presence of pore structure deformation. Most likely, this corresponds to pore cross-sectional area differences,

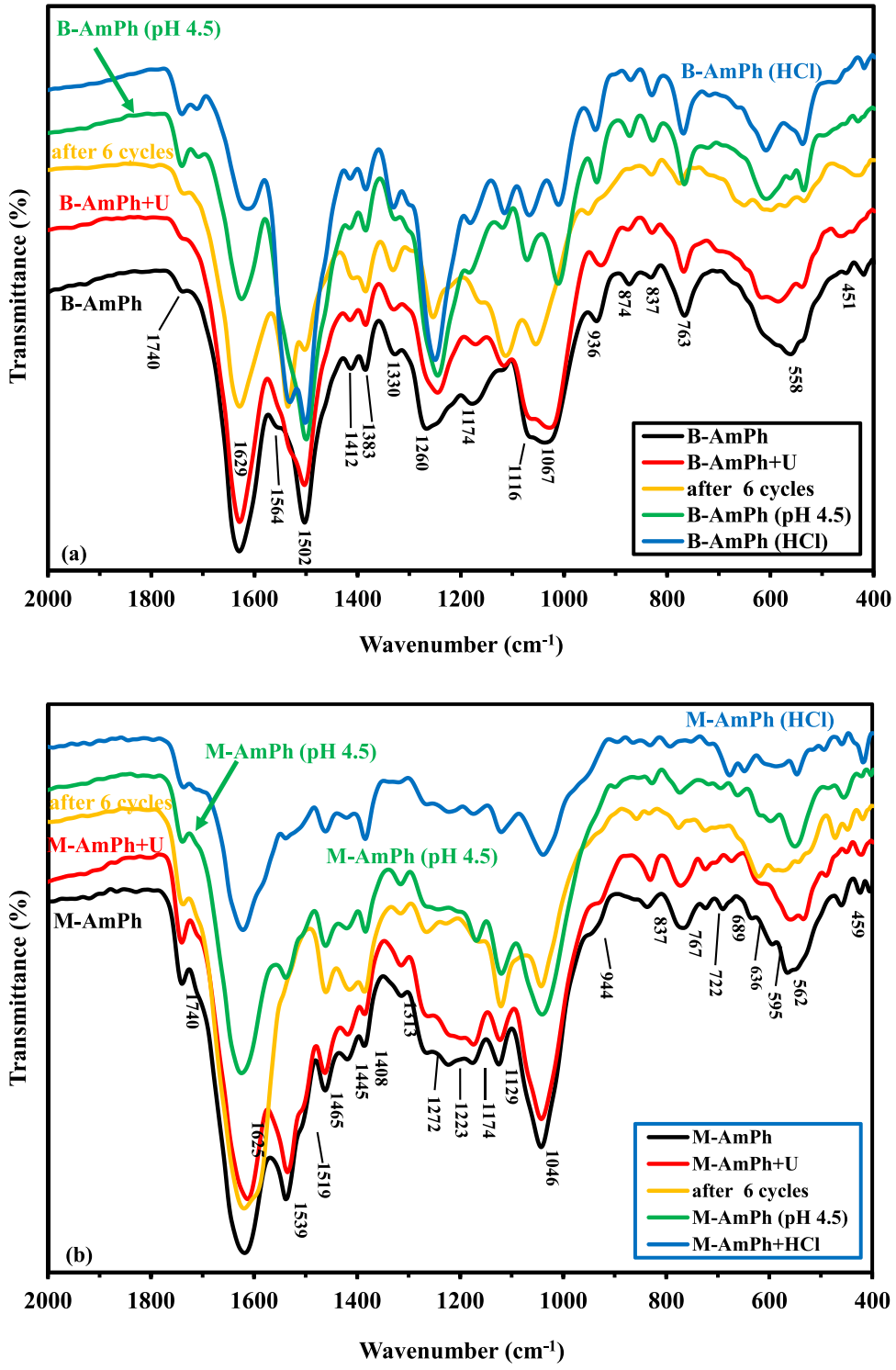

Fig. 1. FTIR spectra of B-AmPh and M-AmPh sorbents (pristine), after contact with pH 4.5 solution and HCl (0.2 M), after U(VI) sorption and 6th step recycling (2000–400 cm^{-1} range).

and/or the presence of pore networking between nearby pores (caused by pore wall faults); this is consistent with the "building" of an interconnected pore structure [35].

The pore size distribution shows a great dispersion for the two sorbents. In the case of M-AmPh, a dual distribution is observed with a class of thin pores (size close to 2.84 nm) and another class centered around 6.06 nm. After complete phosphomethylation, the contribution of the smallest class (around 4.08 nm) to porous volume is considerably reduced and the pore distribution is almost unimodal (around 6.06 nm). The averaged pore size (calculated with the BJH method) decreases from ~8.38 nm for M-AmPh to ~2.28 nm for B-AmPh. The immobilization of the second aminophosphomethyl moiety significantly changes pore dispersion profile and subsequently decreases the pore size. Despite the larger molecular weight and the doubling of functional groups in B-AmPh, the sorbent is more compact because of steric hindrance effects. In any case, the two sorbents can be considered mesoporous materials (pore size being lower than 50 nm, according IUPAC classification).

3.2.6. FTIR analysis

In Fig. 1, the spectra of pristine sorbents are compared with those of:
- pH 4.5-conditioned sorbents,
- sorbents exposed to U(VI) solution (at the same pH),
- after six cycles of desorption, and.
- sorbents exposed to 0.2 M HCl in order (to differentiate the effects of environmental conditions, such as pH or acidity, from the proper interaction with U(VI) and the modifications brought by desorption operation.

The composition of the new sorbents based on the grafting of precursors includes a wide range of functional groups such as -NH-, -NH_2, P = O and –C═S. On the FTIR spectra of B-AmPh and M-AmPh (Fig. 1), these groups and their interactions with UO_2^{2+} can be identified (Fig. S3–full wavenumber range and Table S6). These interactions might be correlated to changes in relative intensity of some peaks, and the appearance, shifting, or disappearance of certain bands [18]. The effective synthesis of aminophosphonate resins by the one pot reaction of thiocarbazide, trimethylphosphite, and p-phthaldehyde is demonstrated by the appearance of specific peaks, such as those of P-based reactive groups. Three series of peaks, have been identified: at 767–763 cm^{-1} for υ(P-CH) bond, at 1272–1260 cm^{-1} for υ(- P = O) [4], and at 1067–1042, 944–936 and 562–558 cm^{-1} (symmetric stretching of P-O-C) [36–38]. Furthermore, the absorption peak appeared at 1330–1313 cm^{-1}, specific to the C═S stretching vibration [39], and the broad band located at 1564–1539 cm^{-1} (assigned to C═C bond, in aromatic rings) confirms the successful synthesis of the α-aminophosphonate materials.

The sorption of U(VI) induces significant changes to the FTIR spectra of the sorbent [11]: the respective intensities of the bands relative to –NH- and –NH_2 decrease (in the region 3456–3440 cm^{-1}). The peaks at 1272–1260, 944–936 and 767–763 cm^{-1} corresponding to vibrations of υ(P = O), υ(P- O- C), and υ(P-CH) are shifted (simultaneously to intensity reduction after metal binding [2]). Notably that, the band located around 1740 cm^{-1} assigned to the υ(-C═O) (in aldehyde) in M-AmPh sorbent has been shifted to 1736 cm^{-1}, while the band at 1223 cm^{-1} corresponding to δ(C-H) (in conjugated aldehyde) is shifted to 1219 cm^{-1}. Relative contributions of amine and phosphonate groups in addition to aldehyde group in the mono sorbent are modified: these groups are involved in metal binding. After uranium sorption, a new band appears at 619 cm^{-1} that is commonly assigned to sulfate groups [1,11].

After six cycles of sorption and desorption, the FTIR spectra of the sorbents were also compared to verify the stability of the materials upon recycling. After desorption, the FTIR spectra (Fig. 1a&b) of metal-loaded sorbents are partially restored to the original spectrum of the sorbents: the peaks are displaced but without totally returning to their original wavenumbers. Marked alterations occur in the regions 3456–3440 cm^{-1} (amine groups) and 1272–763 cm^{-1} (the region where the standard phosphonate bands can be identified). This indicates that the regeneration of the sorbents has a major impact on amine and phosphonate moieties.

3.2.7. XPS analysis

XPS spectroscopy can be used not only for characterizing the materials (identification of specific bonds) but also for identifying their interactions with metals ions after binding. The survey XPS spectrum of B-AmPh and M-AmPh is reported in Fig. 2 (expanded in a wider Binding Energy (BE, eV) range in Fig. S4). The major elements present on the sorbents can be identified: N, O, C, P, and S, as well as sorbed U (when relevant). The high-resolution spectra of these elements (for selected signals) are deconvoluted in Figs. S5and 6; the BE vales, atomic fractions and assignments are reported in Table S7.

The comparison of the deconvoluted signals for M-AmPh and B-AmPh sorbents show significant differences: the phosphomethylation of the second aldehyde group causes significant changes;.

- For C1s signals, little shifts for the 284.22 eV (to 284.46 eV), 285.78 eV (to 286.33 eV) and 287.17 eV (to 287.13 eV) from M-AmPh to B-AmPh respectively, with reflected change of the corresponding atomic fractions; this may be due to the variation of the participation of the functional groups (C-H, C-P, C-S, C-N, and C-O-P).

- In the case of N1s, the M-AmPh sorbent produces two deconvoluted bands with a major signal specified close to 399.77 eV (At, 81.11 %) corresponding to –NH_2, >NH- assignments. While the B-AmPh sorbent produces three deconvoluted bands with a major signal at 400.01 (At 72.28 %) corresponding to C-N assignment.
- For P2p, the presence of both P-O, P-C and protonated phosphonate bonds affirms the phosphomethylation reaction; P2p splits into two convoluted peaks in the M-Sorbent at BEs 132.55 eV and 133.4 eV, which may be specified to $P2p_{3/2}$ (C-P) and ($P2p_{1/2}$ (O-P) with atomic fraction (At) of 42.09 % and 57.91 %, respectively. Whereas P2p exists as one peak in the B-AmPh sorbent at BE 132.73 eV assigned to $P2p_{3/2}$ (C-P).
- O2s signal is relatively stable with a remarkable exception of the peak at 534.17 eV (At 17.33 %) assigned to (O ads·H_2O) in the M-AmPh sorbent which is not observed in B-AmPh sorbent.
- For S2s signals, The S2p signal is relatively stable, with a remarkable exception of the peak at 166.79 eV (At 5.81 %) assigned to (S-O ($2p_{3/2}$) sulfate) in the M-AmPh sorbent which is shifted to 168.46 eV (At 7.92 %) in B-AmPh sorbent.

The XPS analysis of the sorbents after U(VI) sorption are described in detail in (Section D, SI).

3.2.8. pH_{PZC} determination

The pH_{PZC} values provide essential information on sorbent surface charge; making possible anticipating in function of the pH (i.e. the attraction/repulsion forces). The pH_{PZC} as well as the acid-base characteristics of the α-aminophosphonate sorbents (B-AmPh and M-AmPh) were determined using the pH-drift method (Fig. S7) [40]. There are many factors that can determine the acid–base properties of aminophosphonate-based compounds such as: the presence of side functional groups (e.g., NH, NH_2, H-C═O, C═S, P = O), the electronic effects of the different substituents, and the relative molar ratio for phosphonic groups [21].

The pH_{PZC} of M-AmPh is found close to 5.5, this result from the combined effects of the specific acid-base properties of the current reactive groups:

(a) amine groups (with pK_a values ~9.21 for amine groups present in primary amines and ammonia) [41],

(b) thiocarbonyl group (with pK_a values ~10–11),

(c) thiocarbohydrazide (with pK_a value of ~10.58) [42], and.

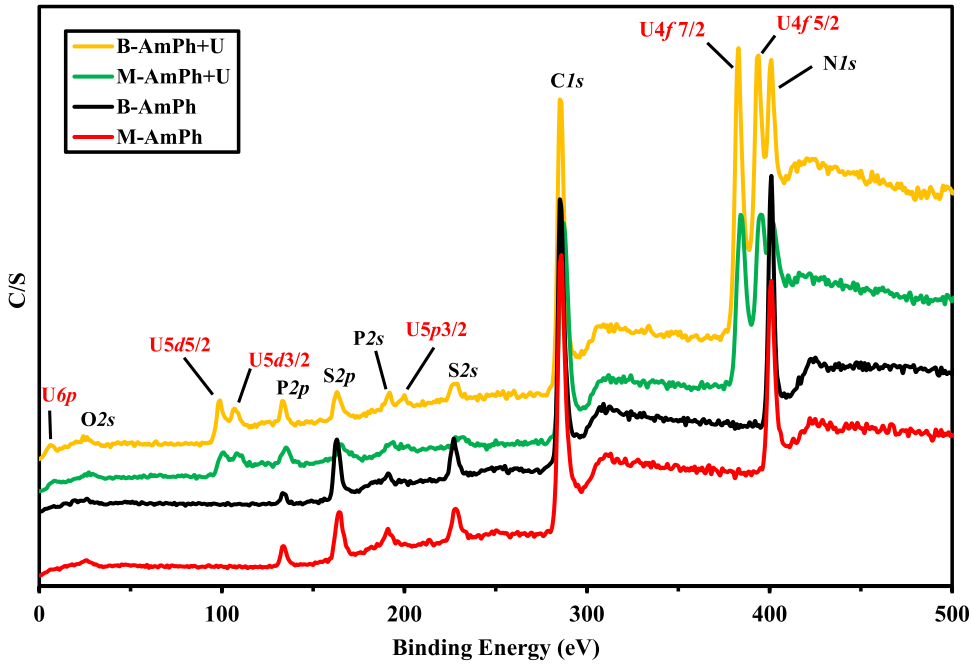

Fig. 2. XPS spectra of M-AmPh and B-AmPh sorbents before and after U(VI) sorption (focused on 0–500 eV Binding Energy range).

(d) phenyl group (with $pK_a \sim 9.93$).

Aminophosphonate-based compounds being mono- and diacids, (with pK_a values of 0.5–1.5 and 5–6, respectively) bring zwitterion effect resulting from the transfer of interior hydrogen from amino groups to P-OH moiety [43]. The pH_{PZC} of B-Am.Ph is slightly higher (~ 6.1). This increase can be attributed to the negative inductive effect (-I) of aldehydic group (in the M-AmPh), which, in turn, reduces the electron density around the phosphonate group and then lowers the pK_a value. Also, the aminophosphomethylation reaction of the second aldehyde group in the B-AmPh introduces extra basic groups such as thiocarbonyl and amino groups to the sorbent. In addition in B-AmPh, the doubling of methyl and amino groups (which have positive inductive effect (+I)) contributes to increase the pH_{PZC} value [21]. Hägele et al. [44] studied the acid-base characteristics of a number of aminophosphonate compounds; they find that the phosphonate group environment has a substantial effect on the pK_a values, which ultimately controls the overall charge of the compound. This is an important criterion for sorption applications since the overall charge may affect attraction or repulsion effects, in relation with operating pH. Despite higher steric hindrance constraints (which could affect acid-base properties, turning down pH_{PZC} value), the other factors (co-existent additional reactive groups) predominantly increase (slightly) the pH_{PZC} value.

3.3. Uranium sorption

3.3.1. pH effect on uranyl U(VI) sorption

The pH is one of the most critical parameters for sorption processes. Indeed, the pH influences the special of metal ions (formation of hydrocolloids, micro-precipitates, hydroxides, and specific complexes), the protonation/deprotonation of reactive groups (overall charge for

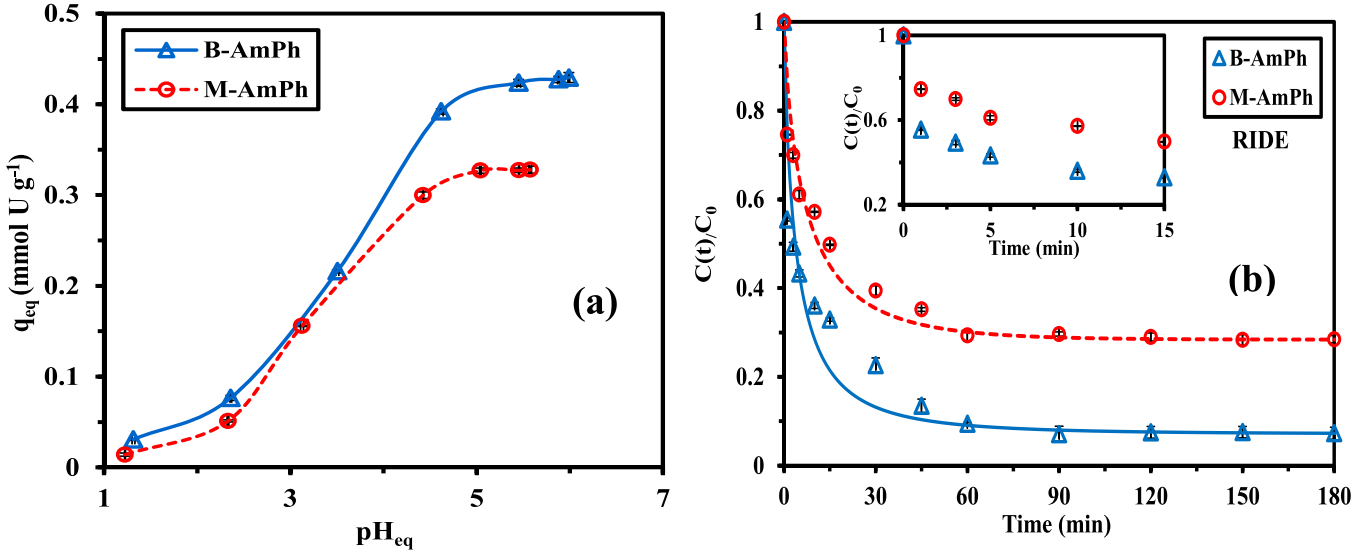

Fig. 3. Effect of pH_{eq} (a) (C_0: 0.21 mmol/L; SD: 0.5 g/L; T: 25 ± 1 °C; time: 120 min; v- 200 rpm), and uptake kinetics (b) – Modeling with the Crank equation (RIDE) (pH_0: 4.5; C_0: 0.21 mmol/L; SD: 0.5 g/L; v- 200 rpm; T: 25 ± 1 °C; insert: initial stage of uptake kinetics – 0–15 min).

attraction/repulsion effects), or sorbent durability [45]. Fig. 3 compares the effect of equilibrium pH on U(VI) sorption capacity for M-AmPh and B-AmPh. Sorption capacities are systematically higher for di-substituted sorbent; however, the increase begins to be significant for pH greater than 4. At pH 5.5 under selected experimental conditions, the sorption capacity increases from 0.33 to 0.42 mmol/g. At pH above 5.5, precipitation mechanisms may occur; meaning overestimation of sorption capacities. At pH below 2.5, the sorption capacities remain negligible (0.05–0.08 mmol/g), the full protonation of reactive groups limits their availability for binding free uranyl ions. Above pH 2.5, the sorption capacity increases almost linearly with the pH up to pH 4.5. Between pH 4.5 and 5.5, the sorption capacity slightly increases and stabilizes to form a plateau. With pH increase, the protonation of reactive groups decreases making possible the complexation of uranyl species and/or their ion exchange with exchangeable protons (on reactive groups). It is noteworthy that for both M-AmPh and B-AmPh in the operable pH range (before precipitation), the surface of the sorbents is globally positively-charged. In addition, B-AmPh having a higher pH_{PZC} value and a higher density of reactive groups, this may explain the stronger sorption of uranyl. The stock solution was prepared by thermal dissolving of uranyl nitrate in concentrated sulfuric acid. This means that uranyl is mainly present in solution (in the studied pH range) as neutral uranyl sulfate species (Fig. S8a); free cationic uranyl (UO_2^{2+}) represents < 32 %, while anionic uranyl sulfate species ($UO_2(SO_4)_2^{2-}$) counts for < 13 % at pH 1 (and < 3 % above pH 2). The sorption proceeds through chelation on phosphate, amine and thiocarbonyl groups with respective contributions depending on the pH (in relation with their respective acid-properties, and attraction/repulsion effects). Under strong acidic conditions, the limitation effect (despite the potential attraction of uranyl species) may be due to the strong competition effect of protons, and the shielding due to the large excess of sulfate anions (Fig. S8b).

The sorption of uranyl onto the sorbents systematically induces an increase of the equilibrium pH (Fig. S9), which is more marked for B-AmPh (because of the higher density of reactive groups that bind more uranyl ions). This pH variation may be explained by proton binding together with uranyl and/or the release of hydroxyl groups (at the higher pH values) because of possible mechanism of ligand exchange at the level of uranyl species. At pH_0 above 5.5–6, the final pH tends to decrease.

The distribution ratio (D) is plotted vs. pH_{eq} in Fig. S10 (log_{10} plot). Below pH_{eq} 5, the data follows a linear trend with a slope close to + 0.5 for the two sorbents. Based on the principle of ion-exchange mechanisms, this would mean that the binding of two uranyl units involves one proton exchange in the global binding mechanism.

3.3.2. Uptake kinetics

The U(VI) uptake kinetics are recorded in Fig. 3 for M-AmPh and B-AmPh. The initial slope of the curve is steep with 50 % of total sorption occurring within 1–3 min of contact (more than 90 % of total sorption is achieved in < 45 min). The equilibrium is reached within 60–90 min of contact. This fast sorption may be explained by the small size of sorbent particles and specific surface area of the sorbents.

The uptake kinetics are usually controlled by a series of mechanisms such as resistance to film diffusion and intraparticle diffusion, and the proper reaction rate of sorption [46–48]. It is commonly accepted that the resistance to external diffusion controls the initial step of the sorption (within the first minutes of contact). The insert in Fig. 3 shows the initial stage and the faster U(VI) sorption with B-AmPh: the higher density of reactive groups improves kinetic speed, despite lower specific surface area and lower pore size). The modeling of kinetic profiles with the models reported in Table S1a; Table 1 reports the parameters of these models and the statistic criteria. The two models that fit better the experimental data are the resistance to intraparticle diffusion (the so-called Crank equation) and the PSOM. The calculated sorption capacity at equilibrium (for the PSOM) is close to experimental values (the deviation is < 3 %). In Fig. 3, the solid lines represent the fitting of experimental profiles with the RIDFE; the fitting of curves with the PFOM and PSOM are reported in Fig. S11. The apparent rate coefficient (for PSOM) k_2 is slightly higher for B-AmPh than for M-AmPh: 1.03 vs. 0.66 min^{-1}, respectively. This is consistent with the observation of the profiles. The effective diffusivity of the uranyl into the sorbents increases from 1.5×10^{-13} m^2/min for B-AmPh to 6.32×10^{-13} m^2/min for M-AmPh. The resistance to intraparticle diffusion plays a significant role in the control of uranium binding; indeed, the self-diffusivity of U(VI) in water is close to 4.56×10^{-8} m^2/min (i.e., five orders higher than the diffusivity in investigated polymers). The decrease in the diffusion properties for the bi-aminophosphonated sorbent can be directly correlated with the reduction in pore size and porous volume (Table S5).

Table 1
U(VI) uptake kinetic using B-AmPh and M-AmPh – Parameters of the models.

Model	Parameter	Unit	B-AmPh	M-AmPh
Experimental	$q_{eq,exp}$	mmol/g	0.428	0.330
PFOM	$q_{eq,1}$	mmol/g	0.393	0.313
	$k_1 \times 10$	min^{-1}	2.68	13.9
	R^2		0.853	0.926
	AIC		-53	-65
PSOM	$q_{eq,2}$	mmol/g	0.416	0.333
	k_2	min^{-1}	1.034	0.664
	R^2		0.930	0.963
	AIC		-64	-76
RIDE	$D_e \times 10^{13}$	m^2/min	1.50	6.32
	R^2		0.929	0.970
	AIC		-63	-78

3.3.3. Sorption isotherms and thermodynamics

In order to evaluate the thermodynamic parameters uranyl sorption isotherms were collected for the two sorbents at pH_0 4.5 at four temperatures ranging between 298 and 328 K. Fig. 4 shows that for both B-AmPh and M-AmPh increasing the temperature increases both the maximum sorption capacity and the initial slope of the isothermal curve. This means that uranyl sorption onto aminophosphonated sorbents is endothermic. The experimental profiles have been modeled with the equations reported in Table S1b. The relevant parameters are listed in Table 2. The quality of the fits is evaluated through the determination coefficient (R^2) and the Akaike information criterion (AIC); the difference in the fit's quality is significant when the $|\Delta(AIC)|>2$. For B-AmPh, the Langmuir is roughly the model the most appropriate for fitting experimental profiles; the sorption capacity is overestimated by 2.7–5.8 %. The solid lines in Fig. 4 represent the Langmuir fit applied to experimental series. The fitting of experimental profiles with the other equations are summarized in Figs. S12 and 13. The Langmuir model assumes that sorption occurs as a monolayer without interactions between sorbed molecules and with homogeneous distribution of binding energies. Despite the diversity of reactive groups (amine, thiocarbonyl and phosphonate moieties), the variability in binding energies does not affect the preference for Langmuir fitting. In the case of M-AmPh, the differences between the different models are less marked, with the remarkable exception of Freundlich equation (which supposes an exponential trend for sorption capacity; herein, the asymptotic trends oppose to this model). The Sips equation is based on the combination of Langmuir and Freundlich equations; despite the introduction of a third-adjustable parameter, the mathematical fitting is not improved. Significant changes in the fitting of experimental profiles are observed while increasing the temperature. At T: 298 K, the Langmuir equation best fits the sorption isotherm (with substantial overestimation of maximum sorption capacity; +16.1 %). At T: 308 K, both Langmuir and D-R equations similarly fit experimental data. At T: 318 K and 328 K, the D-R equation substantially improves the modeling of the isotherms. The D-R equation initially developed for the sorption of gases on porous sorbents was extended to solid/liquid interfaces. The concept is energetically speaking substantially different at the molecular level with solid/gas interface since the solute is surrounded by solvent molecules that cover

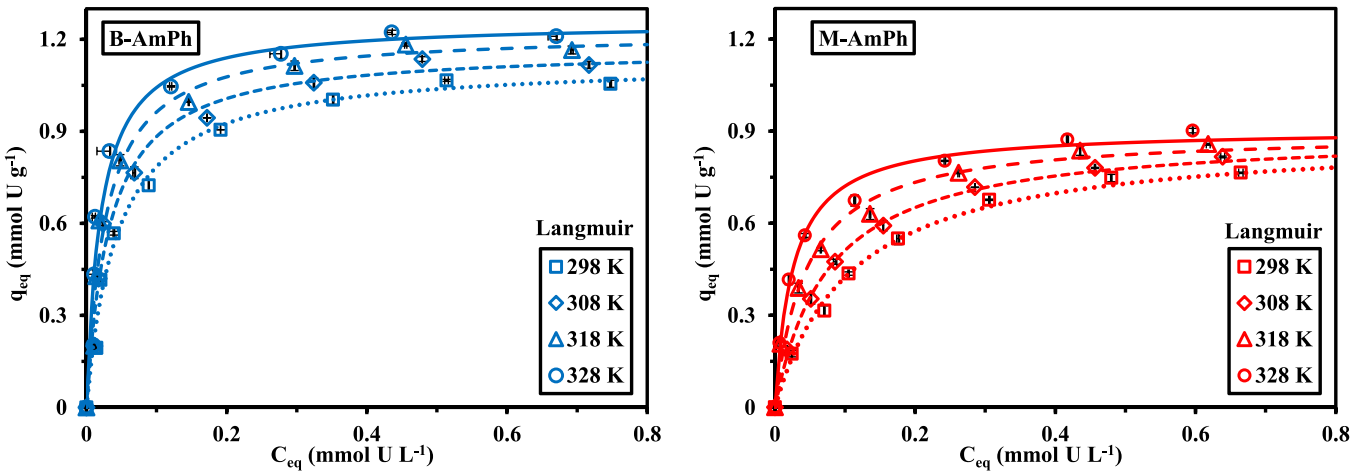

Fig. 4. Sorption isotherms at different temperatures – Modeling with the Langmuir equation (C_0: 0.12–0.28 mmol/L; T: 298–328 K; time: 60 min; v- 200 rpm; SD: 0.5 g/L).

Table 2
U(VI) sorption isotherms using B-AmPh and M-AmPh – Parameters of the models.

Model	Param.	Unit	B-AmPh				M-AmPh			
			298 K	308 K	318 K	328 K	298 K	308 K	318 K	328 K
Experimental	$q_{m,exp}$	mmol/g	1.066	1.136	1.183	1.223	0.765	0.816	0.858	0.902
Langmuir	$q_{eq,L}$	mmol/g	1.128	1.171	1.223	1.256	0.888	0.896	0.896	0.907
	b_L	L/mmol	22.8	30.6	37.0	48.8	9.14	13.3	22.5	38.8
	R^2	-	0.989	0.981	0.975	0.959	0.994	0.998	0.993	0.992
	AIC	-	-52	-46	-43	-38	-68	-72	-49	-58
Freundlich	k_F	(mmol/g)/(mmol/L)^{n_F}	1.267	1.349	1.419	1.470	0.878	0.928	0.969	1.014
	n_F	-	3.63	3.84	4.030	4.318	3.062	3.430	4.032	4.531
	R^2	-	0.941	0.932	0.932	0.895	0.952	0.960	0.965	0.961
	AIC	-	-37	-35	-32	-29	-45	-46	-43	-45
Sips	$q_{eq,S}$	mmol/g	1.126	1.161	1.172	1.198	0.858	0.911	1.013	0.985
	b_S	(mmol/L)^{n_S}	23.5	35.1	97.4	211	12.23	11.4	7.22	12.9
	n_S	-	0.993	0.969	0.817	0.755	0.912	1.049	1.416	1.338
	R^2	-	0.989	0.981	0.977	0.962	0.995	0.998	0.997	0.997
	AIC	-	-47	-42	-37	-33	-61	-68	-48	-62
Temkin	A_T	L/mol	301	430	554	849	108	185	501	891
	b_T	J.kg/mol^2	11761	12144	12373	13131	13794	15039	17785	18971
	E_T	kJ/mol	11.0	10.0	10.5	10.7	18.0	18.4	20.7	21.0
	R^2	-	0.977	0.968	0.952	0.931	0.983	0.989	0.991	0.990
	AIC	-	-46	-42	-37	-33	-55	-58	-50	-57
D-R	q_{DR}	mmol/g	1.147	1.208	1.270	1.313	0.845	0.876	0.898	0.934
	$k_{DR} \times 10^8$	mol^2/J^2	1.199	0.979	0.839	0.692	1.953	1.452	0.985	0.732
	E_{DR}	kJ/mol	9.13	10.1	10.9	12.0	7.16	8.30	10.1	11.7
	R^2	-	0.986	0.976	0.964	0.945	0.995	0.998	0.998	0.997
	AIC	-	-50	-45	-40	-35	-65	-74	-53	-67

the entire surface [49]. The sorption of solute molecules requires breaking molecular interactions solute/solvent and at solid/solvent levels; this makes the interpretation of energetic parameters debatable for distinguishing chemical and physical sorption. Herein, the typical E_{DR} energy parameter increases with temperature but remain below 12 kJ/mol, which is assigned to physical adsorption mechanism [50]. However, Puccia et al. [49] clearly demonstrated that the limit value and debatable in the case of solid/liquid systems. The Temkin equation supposes that the sorption occurs as a multi-layer and that the heat of sorption linearly decreases with surface coverage [51]. Herein, the Temkin equation cannot correctly fit experimental data; best results were obtained with M-AmPh at the highest temperatures (though AIC values remained lower than the values reached with D-R models). Basically, the A_T parameter is higher for B-AmPh (301–430 L/mol) sorbent (compared with M-AmPh;108–185 L/mol) at low temperatures; at higher temperatures the constants tend to similar values. On the opposite hand, the energy parameter of Temkin equation (b_T) is systematically higher for M-AmPh (13.8–19.0 kJ.kg/mol^2) than for B-AmPh (11.8–13.1 kJ.kg/mol^2).

Based on the Langmuir affinity coefficient (b_L), the thermodynamic parameters were calculated (Section E, SI). Fig. S14 shows the van't Hoff plots for U(VI) sorption using B-AmPh and M-AmPh. The thermodynamic parameters are strongly influenced by the extent of aminophosphonation. With increasing the number of aminophosphonate incorporated into the sorbent, both the enthalpy and entropy changes decrease (Table S8): from 39.4 to 20.1 kJ/mol and from 207 to 151 J/mol.K, respectively. The positive values of enthalpy confirm the endothermic sorption of uranyl. The positive values of the entropy change demonstrate that the disorder of the system (increase in randomness) follows the sorption of uranyl ions onto the sorbents; the degree of freedom of solute molecules increases [9]. The negative values of the Gibbs free energy (ΔG°) mean that the sorption process is spontaneous. In addition, the values of $|T \times \Delta S^\circ|$being systematically higher than those of$|\ \Delta G^\circ|$, the sorption of uranyl on aminophosphonate sorbents is entropically driven. Duan et al. [52] reported spontaneous and endothermic sorption of uranium with hierarchically porous metal-organic

frameworks; however, the enthalpy change (132 kJ/mol) and the entropy change (496 J/mol.K) are significantly higher than the values obtained with aminophosphonate-based sorbents. On the opposite hand, for U(VI) sorption onto amidoximated MCM-41 sorbent, the enthalpy change is lower (~10.3 kJ/mol) while entropy change is of the same order (~124 J/mol.K) [53].

The higher sorption of uranyl by B-AmPh can be explained by the higher density of reactive groups (compared with M-AmPh). The comparison of maximum sorption capacities (at the four temperatures) shows that the bis-aminophosphonation increases the sorption by 36–39 %. This is higher than the relative ratios for N, P, and S elements ($N_{B\text{-}AmPh}/N_{M\text{-}AmPh}$, and so on), which range between 1.16 and 1.28 (only 0.94 for $O_{B\text{-}AmPh}/O_{M\text{-}AmPh}$). The enhancement of sorption performance is not only due to the density of reactive groups; probably some other parameters may explain this improvement (acid-base property, more favorable arrangement of reactive groups).

The favorability of sorption is usually evaluated through the dimensionless parameter RL calculated using $R_L = (1 + (b_L \times C_0))^{-1}$ (not shown). The value of R_L decreases with increasing the initial concentration and increasing the temperature for both B-AmPh and M-AmPh. For the different systems, the parameter is below 0.5 (i.e., lower than the threshold (1) for discriminating between favorable and unfavorable systems). Uranyl sorption is favorably sorbed onto the aminophosphonate-based sorbent, and the favorability increases with increasing the temperature and metal concentration.

Table S9 compares the U(VI) sorption performances of a series of alternative sorbents (including main experimental conditions) with the values reached with B-AmPh and M-AmPh. Some sorbents bearing amidoxime groups show outstanding sorption properties [54,55] (i.e. maximum sorption capacities in the range 1.78–2.18 mmol/g; and affinity coefficients in the range 30–164 L/mmol). Zhu et al. [56] also reported remarkable sorption capacities (2.5 mmol/g) in the case of mixed Ni/Mn LDH deposited onto carbonized polymer matrices. In the case of phosphonate-based sorbents including aminophosphonate sorbents, the sorption capacities are of the same order of magnitude (1.057–1.45 mmol/g; [4,5,13,20,57]) than the maximum reached with B-AmPh (i.e., 1.07 mmol/g). These results show that B-AmPh (better than M-AmPh) is on line with the best phosphonate-functionalized sorbents.

3.3.4. *Metal binding mechanism*

FTIR and XPS data are used together with the pHs to elucidate the binding mechanisms; different uranium sorption modes were employed (Scheme2) based on these analyses before and after U(VI) sorption. Based on the proposed structures of the two sorbents shown in Scheme 1, the functional groups available for U(VI) binding are primary and secondary amine, thiocarbonyl and phosphonate, groups. The complexation binding mechanisms of U(VI) with the two aminophosphonate sorbents through the different heteroatoms may involve:

(I) two coordinating bonds, with O-atom of the phosphonate group (P = O) and N-atom of >NH group at connection (linkage) point.
(II) two coordinating bonds with >NH group (secondary amine) at connection point and thiocarbonyl group (C=S) of the thiocarbazide.
(III) two coordinating bonds within the thiocarbazide molecule via the thiocarbonyl group (C=S) and the terminal $–NH_2$ group.
(IV) two coordinating bonds, with O-atoms of the –OMe groups from phosphonate groups.
(V) two coordinating bonds, via the two secondary amine groups within the thiocarbazide molecule.

As a result, contribution mode (IV&V) produces an unstable four-membered ring, while modes (I-III) produce stable five-membered chelating rings. The stability of the produced complex is enhanced by increasing the number of chelate rings, and as a result, the sorption capacity for metal improves. Moreover, the amine groups of the thiocarbazide moiety have an ion-exchange mechanism that may be affected by the pH through protonation/deprotonation as well as uranyl speciation; the suspected anion-exchange reactions are poorly probable: Overall ion-exchange reaction:

$$\left(R_2NH_2^+\right)_2SO_4^{2-} + UO_2(SO_4)_2^{2-} \leftrightarrow \left(R_2NH_2^+\right)_2UO_2(SO_4)_2^{2-} + SO_4^{2-} \quad (5a)$$

For the sorption of neutral sulfate species, a different mechanism–namely molecular addition mechanism (Eq.5b)–was anticipated to work as follows:

$$\left(R_2NH_2^+\right)_2SO_4^{2-} + UO_2SO_4 \leftrightarrow \left(R_2NH_2^+\right)_2UO_2(SO_4)_2^{2-} \quad (5b)$$

The total sorption capacities were the sum of the both chelation and ion-exchange mechanisms (which controlled the sorption process). As the tentative complexation mechanisms and interaction modes between U(VI) ion and reactive groups on both sorbents were illustrated in Scheme 2, also the equations 5a&b showed the possible mechanisms for ion-exchange in the case of anionic uranyl sulfate species as well as molecular addition mechanism for neutral uranyl sulfate species.

3.3.5. *Metal desorption and sorbent recycling*

The design of competitive sorbent requires demonstrating the possibility to valorize sorbed metal (by effective desorption with high concentrating effect) and by proved recyclability of the sorbent (with high stability of sorption and desorption performances). Sodium bicarbonate solutions was used for uranium elution from aminophosphonate-based sorbents [2] or strong base anion exchange resins (PFA4759) [58].

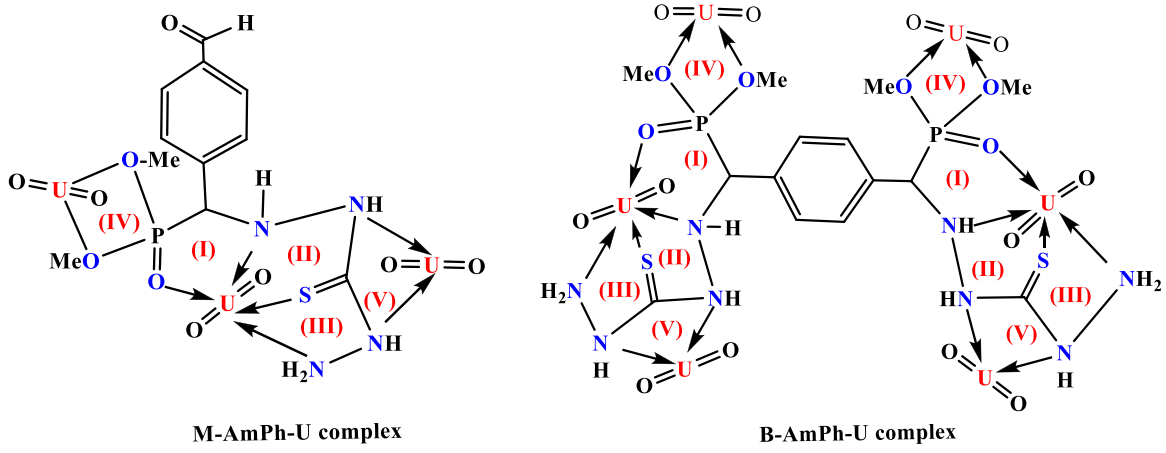

Scheme 2. Tentative complexation mechanisms and interaction modes between U(VI) and reactive groups on both sorbents.

The sorption of U(VI) onto aminophosphonate-based sorbents being very sensitive to pH (with limited sorption capacity in acidic solutions), the use of an acid eluent for metal elution from saturated sorbent is a logical way for proceeding to the regeneration of the sorbent. Preliminary tests showed that 0.2 M HCl as well as 0.25 M $NaHCO_3$ solution were efficient for uranium recovery (the desorption efficiency ≥98 %, for first cycle for both sorbents), Moreover, the 0.2 M HCl showed faster kinetics 60 min over 90 min of contact for $NaHCO_3$.

Herein,0.0.2 M HCl solutions were successfully used. Liu et al. [59] used higher HCl concentration (1 M.HCl) for uranium desorption from functionalized fungus-based sorbent. In the case of hydroxypyridone functionalized polyethylene nonwoven fabrics, Zhang et al. [60] carried out uranium elution with 1 M HCl solution; they reached full desorption of the metal.

Table S10 compares the sorption and desorption performances (efficiencies, %) for six successive cycles. The efficiencies of both sorption and desorption slightly and progressively decrease with the number of cycles. It is noteworthy that metal desorption is not complete, meaning that the metal progressively saturates the sorbents and decreases the availability of reactive groups for further sorption steps. It is noteworthy that the loss is sorption and desorption efficiencies are weakly less marked for B-AmPh sorbent (7.0 % in sorption, 4.4 % in desorption) (compared to 8.9 % and 5.9 % for M-AmPh). The bis-phosphonation sorbent maintains a greater density of functional groups available for

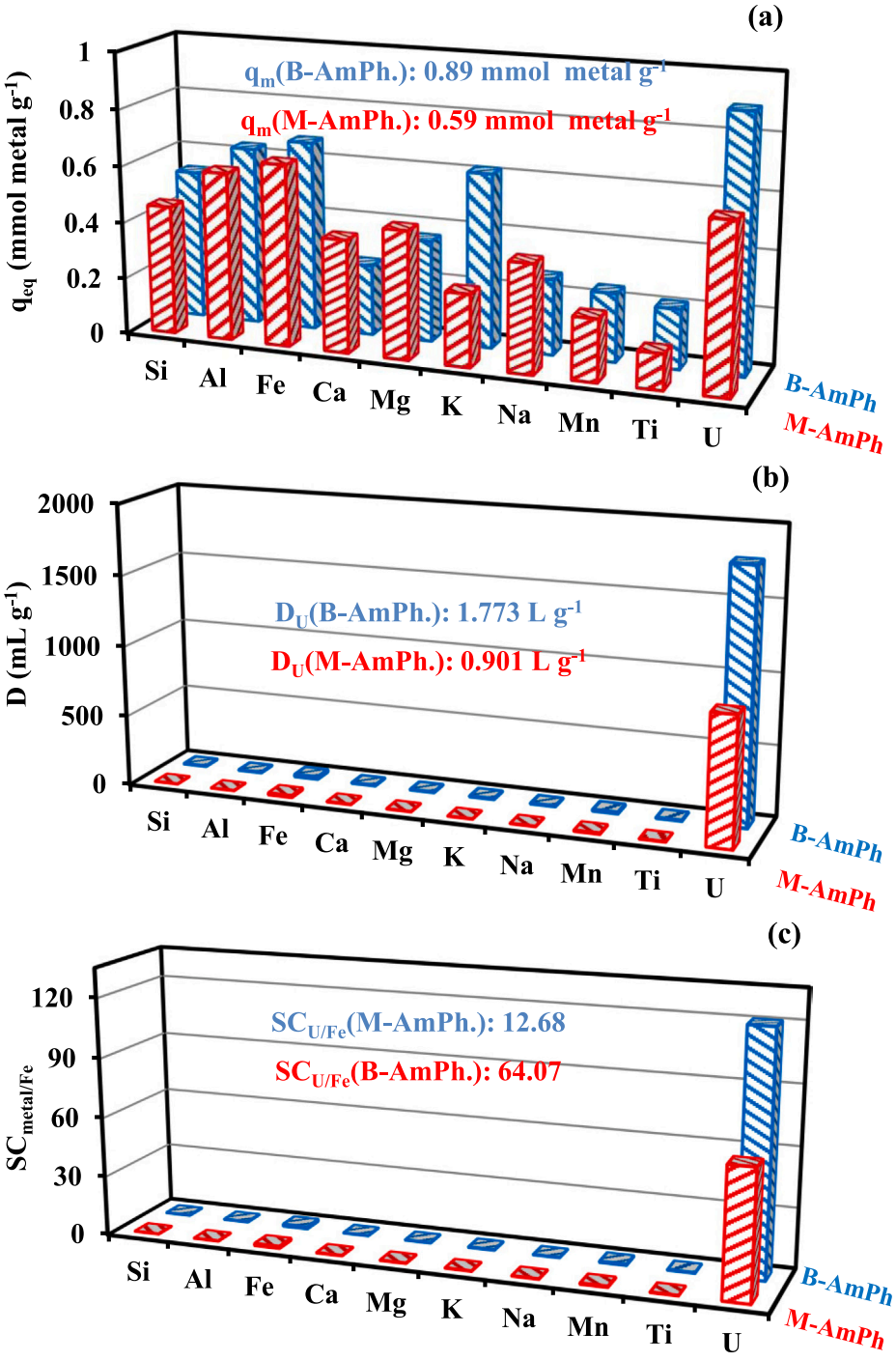

Fig. 5. Metal sorption from PPLS – (a) sorption capacities, (b) distribution ratios, and (c) $SC_{metal/Fe}$) (pH_0: 4.5; SD: 0.5 g/L; time: 60 min; T: 25 ± 1 °C; v- 200 rpm).

U(VI) binding, that explain the limited impact of recycling on global performance. These performances are comparable with those reported for other systems. For uranium desorption from phosphorylated hyper corss-linked polymers, using HNO_3 solutions, Tian et al. [33] also reported a progressive decrease in sorption that reaches up to 25 % at the third cycle. In the case of amine-functionalized SBA-15 sorbent, the loss in sorption at the fourth cycle was 12 % (using sodium carbonate as the eluent) [54]. Han et al. [61] reported a loss of 13 % at the fifth cycle for U(VI) desorption from amidoximated marine fungus (using 0.1 M HCl), with a decrease in desorption efficiency close to 15 %. Similar loss (around 13 % at the fifth cycle) is also reported by Liu et al. [59] in the release of U(VI) from amidoximated fungal-based sorbent with 1 M HCl solutions. These data confirm the potential of the sorbents (especially the bis-aminophosphonated material) for recycling and efficient metal recovery. This should be confirmed in the treatment of real effluents to check the effect of competitor or inhibiting compounds on both sorption and desorption performances.

3.3.6. *Application of sorbents for the treatment of ore leachates – selectivity issues*

Fig. 5 compares the sorption of the different metal ions (and metalloids) for both B-AmPh and M-AmPh through three indicators: sorption capacity at equilibrium (q_{eq}, a), distribution ratio (D, b), and selectivity coefficient ($SC_{metal/Fe}$, c). The selectivity coefficient is defined as:

$$SC_{metal/Fe} = \frac{D_{metal}}{D_{Fe}} = \frac{q_{eq,metal} \times C_{eq,Fe}}{C_{eq,metal} \times q_{eq,Fe}} \quad (2)$$

Fe was selected being the highest distribution ratio after U; this allows illustrating the remarkable capacity of the sorbents to extract U from complex effluent.

Despite the huge excess of competitor ions, the sorption capacities for U(VI) remains very high (0.59 and 0.89 mmol/g for B-AmPh and M-AmPh, respectively), and generally higher than the values reached for other metals (except for Fe, where the sorption capacity with M-AmPh is slightly higher) (Fig. 5a). It is noteworthy that B-AmPh shows the same differential with M-AmPh for complex solution and synthetic single-component solution. Despite the complexity of the solution, and the simultaneous sorption of other metals, the decrease in maximum sorption does not exceed 16 % for bis-aminophosphonated sorbent and up to 23 % for mon-grafted sorbent. The distribution ratio for U(VI) attains 1.77 L/g for B-AmPh, almost twice the value for M-AmPh (Fig. 5b); however, these values are drastically higher than those of the other metals (or metalloid): around 14 mL/g for Fe(III), while for the other elements the D values range between 0.33 and 8.08 mL/g. This means that the sorbents (especially B-AmPh) strongly enrich uranium in the solid phase (compared with its actual fraction in the liquid phase). The preference of the sorbents for U(VI) is confirmed by Fig. 5c: the selectivity coefficients for U against Fe reaches 64 and 120 for B-AmPh and M-AmPh. The large differences in the relative initial concentrations makes the comparison difficult; however, the order of magnitude clearly shows that the sorbents have a strong affinity and selectivity for U(VI) against other metal (and metalloid) cations. The double aminophosphonation is notably more efficient for the selective separation of uranyl ions from complex effluent.

It is noticeable that the cumulative sorption capacities for B-AmPh and M-AmPh reach up to 5.35 and 4.44 mmol/g; this is significantly higher than the maximum sorption capacity obtained at saturation with single-component U(VI) solutions. Both the huge concentrations of co-metal ions and their binding on other functional groups may explain this substantial increase.

The selectivity of a sorbent may be influenced by a multiplicity of factors. According to Pearson's rules (the HSAB principles) uranyl is considered a hard acid, which is supposed to prefer binding to ligands bearing hard bases according: N > P and O>S [14]. It is noteworthy that all the major elements present in the PPLS are member of the hard acids (similar to uranyl); this means that the HSAB principles alone cannot explain the remarkable selectivity of the sorbents for U(VI). On the other hand, base metals (present as traces) such as Ni(II), Co(II), Cu(II) or Zn (II) are borderline metal ions; which are expected to have lower affinity for N- and O- bearing ligands. The remarkable binding of Cu(II) (not analyzed but appearing in the semi-quantitative EDX analysis of PPLS-loaded sorbents, Fig. S15) may be explained by interactions with alternative groups.

This preference can be modulated by the (+I) and (-I) inductive effects of phosphonate functional groups, which may turn up (thiocarbonyl and amine groups) or down (aldehyde groups) the ability of the functional groups to bind uranyl ions. The steric hindrance may cause some limitations in terms of accessibility; on the opposite hand, the arrangement may help in activating cooperative binding with vicinal reactive groups. This is apparently the case in the current context: despite lower specific surface area, smallest pores, bis-aminophosphonated sorbent shows higher sorption capacity and greater selectivity for uranium. The relative contributions of these different mechanisms are difficult to evaluate. Hermann and Lukes [62] studied the binding properties of a variety of phosphonodipepetides bearing various functional groups for divalent cations (Ni(II), Co(II), Zn (II) and Cu(II)). They described the contribution of the steric hindrance as well as the deprotonation characteristics of the amino acid side chains. Nevertheless, it is reported that the phosphonic groups having high complexing capability can modulate these factors effect more than the classical dipeptides.

The metal-loaded sorbents (after contact with PPLS) were eluted using 0.2 M HCl solutions. The desorption reached 92 % and 89 % for B-AmPh and M-AmPh, respectively. This is weakly lower than for single-component U(VI)-loaded (Table S10). The presence of other metals loaded on the sorbent can explain this little decrease. Changing the concentration of the acid or the solid/liquid ratio could be a solution for enhancing uranyl release. The valorization of uranium can be operated by precipitation with ammonium hydroxide (Section F.4, SI). The U concentrate produced contain substantial impurities (10.4 % for B-AmPh and 22.7 % for M-AmPh): the impurities are constituted of iron and potassium (almost equally, around 5–6 % each), with a supplementary impurity in the case of M-AmPh (copper is also found in the U concentrate at substantial level: ~10 %).However the presence of other elements and metals at significant level; these levels probably exceed the levels accepted for U concentrate on commercial market. It could have been interesting proposing purification techniques for reaching commercial levels.

4. Conclusion

The synthesis of sorbents based on α-aminophosphonates, which are generally-speaking good metal-complexing agents, reveals efficient for designing a selective sorbent for uranium (as demonstrated by uranium recovery from acidic leachate of complex ore). The one-pot synthesis of two aminophosphonate derivatives proceeds by direct reaction of thiocarbazide, trimethylphosphite, and p-phthaldehyde. With changing the molar ratio between thiocarbazide/trimethylphosphite (equimolar) and p-phthaldehyde it is possible producing two sorbents with different textural properties, and different content of reactive groups. FTIR and XPS analyses confirm the contribution of amine, thiocarbonyl, and phosphonate moieties in the binding of U(VI). The bis-aminophosphonated sorbents shows slightly higher sorption capacity at the optimum pH (around 4.5), better desorption property (using 0.2 M HCl solution as the eluent) and greater stability at recycling than the mono-aminophosphonated material. The mass transfer properties are slightly depleted (for bis-aminophosphonated sorbent) due to weaker porosity characteristics (steric hindrance). The kinetic profiles can be fitted by the pseudo-second order rate model and the resistance to intraparticle diffusion (the so-called Crank equation). The bis-aminophosphonation increases the maximum sorption capacity by ~39 % (from 0;765–1.066 mmol/g), at T: 25 ± 1 °C (only 23 % at T: 55

± 1 °C, from 0.902 to 1.223 mmol/g). The sorption isotherms are best fitted by the Langmuir equation in the case of B-AmPh, while for M-AmPh the Dubinin-Radushkevich best model experimental profiles (especially at higher temperatures). Another advantage of increasing the density of reactive groups concerns the enhanced selectivity of the sorbent for U(VI). Indeed, in the treatment of acidic leachate of Egyptian ore, which contains large excess of alkaline and alkali-earth metals (in addition to other major elements such as silica and iron), B-AmPh shows significantly greater selectivity for U(VI) than M-AmPh. Despite the huge excess of co-metal ions, the sorption capacities are only reduced by 16 % and 23 % compared with synthetic single-component U(VI) solutions for B-AmPh and M-AmPh, respectively. The cumulative sorption capacities reached quite high values (5.35 and 4.44 mmol/g, respectively); meaning that the strong sorption of other metals (favored by high concentrations) weakly limits U(VI) sorption and that the binding of these metals may involve other reactive groups. However, the high concentrations of these co-ions do not allow reaching high-purity U concentrate (after metal elution from the sorbent and ammonium hydroxide precipitation).

Credit authorship contribution statement

Enas A. Imam: Methodology, Investigation, Formal analysis, Data curation, Writing-original draft. **Ahmed I. Hashem, Ibrahim El-Tantawy ElSayed and Mohammad G. Mahfouz:** Conceptualization, Supervision, Validation, Writing-review & editing, **Ahmed A. Galhoum and Ahmad A. Tolba**: Conceptualization, Supervision, Visualization, Data curation, Writing-review & editing. **Ahmed I. El-Tantawy:** Methodology, Formal analysis, Investigation. **Eric Guibal:** Conceptualization, Software, Formal analysis, Data curation, Writing-review & editing.

Declaration of Competing Interest

The authors declare that they have no known competing financial interests or personal relationships that could have appeared to influence the work reported in this paper.

Data Availability

No data was used for the research described in the article.

Acknowledgements

Authors acknowledge Nuclear Materials Authority (Egypt) for their support. Special dedication to the memory of Prof. Ahmed Donia.

Appendix A. Supporting information

Supplementary data associated with this article can be found in the online version at doi:10.1016/j.jece.2023.109951.

References

[1] A.A. Al-Ghamdi, A.A. Galhoum, A. Alshahrie, Y.A. Al-Turki, A.M. Al-Amri, S. Wageh, Mesoporous magnetic cysteine functionalized chitosan nanocomposite for selective Uranyl ions sorption: experimental, structural characterization, and mechanistic studies, Polymers 14 (13) (2022), https://doi.org/10.3390/polym14132568.

[2] M.M. Rashad, I.E. El-Sayed, A.A. Galhoum, M.M. Abdeen, H.I. Mira, E.A. Elshehy, S. Zhang, X. Lu, J. Xin, E. Guibal, Synthesis of α-aminophosphonate based sorbents – Influence of inserted groups (carboxylic vs. amine) on uranyl sorption, Chem. Eng. J. 421 (2021), 127830, https://doi.org/10.1016/j.cej.2020.127830.

[3] Y. Xie, C. Chen, X. Ren, X. Wang, H. Wang, X. Wang, Emerging natural and tailored materials for uranium-contaminated water treatment and environmental remediation, Prog. Mater. Sci. 103 (2019) 180–234, https://doi.org/10.1016/j.pmatsci.2019.01.005.

[4] E.A. Imam, I. El-Tantawy El-Sayed, M.G. Mahfouz, A.A. Tolba, T. Akashi, A. A. Galhoum, E. Guibal, Synthesis of α-aminophosphonate functionalized chitosan sorbents: Effect of methyl vs phenyl group on uranium sorption, Chem. Eng. J. 352 (2018) 1022–1034, https://doi.org/10.1016/j.cej.2018.06.003.

[5] X. Liu, J. Li, X. Wang, C. Chen, X. Wang, High performance of phosphate-functionalized graphene oxide for the selective adsorption of U(VI) from acidic solution, J. Nucl. Mater. 466 (2015) 56–64, https://doi.org/10.1016/j.jnucmat.2015.07.027.

[6] C. Yawen, W. Chunfang, Z. Liu, L. Zhang, L. Chen, J.-Q. Wang, X. Wang, S. Yang, S. Wang, Fabrication of phosphorylated graphene oxide-chitosan composite for highly effective and selective capture of U(VI), Environ. Sci.: Nano 4 (2017), https://doi.org/10.1039/C7EN00412E.

[7] B. Mahanty, P.K. Mohapatra, Highly efficient separation of thorium from uranium in nitric acid feeds by solid phase extraction using Aliquat 336, Purif. Technol. 237 (2020), 116318, https://doi.org/10.1016/j.seppur.2019.116318.

[8] A. Rahmati, A. Ghaemi, M. Samadfam, Kinetic and thermodynamic studies of uranium(VI) adsorption using Amberlite IRA-910 resin, Ann. Nucl. Energy 39 (1) (2012) 42–48, https://doi.org/10.1016/j.anucene.2011.09.006.

[9] J. Bai, X. Ma, H. Yan, J. Zhu, K. Wang, J. Wang, A novel functional porous organic polymer for the removal of uranium from wastewater, Microporous Mesoporous Mater. 306 (2020), 110441, https://doi.org/10.1016/j.micromeso.2020.110441.

[10] A.A. Galhoum, W.H. Eisa, I. El-Tantawy El-Sayed, A.A. Tolba, Z.M. Shalaby, S. I. Mohamady, S.S. Muhammad, S.S. Hussien, T. Akashi, E. Guibal, A new route for manufacturing poly(aminophosphonic)-functionalized poly(glycidyl methacrylate)-magnetic nanocomposite - Application to uranium sorption from ore leachate, Environ. Pollut. 264 (2020), 114797, https://doi.org/10.1016/j.envpol.2020.114797.

[11] M.K. Sureshkumar, D. Das, M.B. Mallia, P.C. Gupta, Adsorption of uranium from aqueous solution using chitosan-tripolyphosphate (CTPP) beads, J. Hazard. Mater. 184 (1) (2010) 65–72, https://doi.org/10.1016/j.jhazmat.2010.07.119.

[12] S.S. Lee, W. Li, C. Kim, M. Cho, J.G. Catalano, B.J. Lafferty, P. Decuzzi, J. D. Fortner, Engineered manganese oxide nanocrystals for enhanced uranyl sorption and separation, Environ. Sci. Nano 2 (5) (2015) 500–508, https://doi.org/10.1039/C5EN00010F.

[13] L.-Y. Yuan, Y.-L. Liu, W.-Q. Shi, Y.-L. Lv, J.-H. Lan, Y.-L. Zhao, Z.-F. Chai, High performance of phosphonate-functionalized mesoporous silica for U(vi) sorption from aqueous solution, Dalton Trans. 40 (28) (2011) 7446–7453, https://doi.org/10.1039/C1DT10085H.

[14] R.G. Pearson, Hard and soft acids and bases, J. Am. Chem. Soc. 85 (22) (1963) 3533–3539, https://doi.org/10.1021/ja00905a001.

[15] A. Amira, Z. Aouf, H. K'tir, Y. Chemam, R. Ghodbane, R. Zerrouki, N.-E. Aouf, Recent advances in the synthesis of α-aminophosphonates: a review, ChemistrySelect 6 (24) (2021) 6137–6149, https://doi.org/10.1002/slct.202101360.

[16] D.A. Elsherbiny, A.M. Abdelgawad, M.E. El-Naggar, R.A. El-Sherbiny, M.H. El-Rafie, I.E.-T. El-Sayed, Synthesis, antimicrobial activity, and sustainable release of novel α-aminophosphonate derivatives loaded carrageenan cryogel, Int. J. Biol. Macromol. 163 (2020) 96–107, https://doi.org/10.1016/j.ijbiomac.2020.06.251.

[17] R.R. Neiber, A.A. Galhoum, I. El-Tantawy El Sayed, E. Guibal, J. Xin, X. Lu, Selective lead (II) sorption using aminophosphonate-based sorbents: effect of amine linker, characterization and sorption performance, Chem. Eng. J. 442 (2022), 136300, https://doi.org/10.1016/j.cej.2022.136300.

[18] H. Fernández-Pérez, P. Etayo, A. Panossian, A. Vidal-Ferran, Phosphine−phosphinite and phosphine−phosphite ligands: preparation and applications in asymmetric catalysis, Chem. Rev. 111 (3) (2011) 2119–2176, https://doi.org/10.1021/cr100244e.

[19] W. Tang, X. Zhang, New chiral phosphorus ligands for enantioselective hydrogenation, Chem. Rev. 103 (8) (2003) 3029–3070, https://doi.org/10.1021/cr020049i.

[20] Y. Ren, R. Yang, L. Shao, H. Tang, S. Wang, J. Zhao, J. Zhong, C. Kong, The removal of aqueous uranium by SBA-15 modified with phosphoramide: a combined experimental and DFT study, RSC Adv. 6 (73) (2016) 68695–68704, https://doi.org/10.1039/C6RA12269H.

[21] V.P. Kukhar, V.D. Romanenko, Chemistry of aminophosphonic acids and phosphonopeptides, amino acids, peptides and proteins in organic chemistry, Wiley-VCH Verl. GmbH C. KGaA Weinh. (Ger.) (2009) 189–260, https://doi.org/10.1002/9783527631780.ch5.

[22] J. Muller, B. Prelot, J. Zajac, S. Monge, Synthesis and study of sorption properties of polyvinyl alcohol (PVA)-based hybrid materials, React. Funct. Polym. 144 (2019), 104364, https://doi.org/10.1016/j.reactfunctpolym.2019.104364.

[23] S.D. Alexandratos, X. Zhu, M. Florent, R. Sellin, Polymer-supported bifunctional amidoximes for the sorption of uranium from seawater, Ind. Eng. Chem. Res. 55 (15) (2016) 4208–4216, https://doi.org/10.1021/acs.iecr.5b03742.

[24] Y. Zhou, Y. Gao, H. Wang, M. Xia, Q. Yue, Z. Xue, J. Zhu, J. Yu, W. Yin, Versatile 3D reduced graphene oxide/poly(amino-phosphonic acid) aerogel derived from waste acrylic fibers as an efficient adsorbent for water purification, Sci. Total Environ. 776 (2021), 145973, https://doi.org/10.1016/j.scitotenv.2021.145973.

[25] S. Zhu, M. Xia, Y. Chu, M.A. Khan, W. Lei, F. Wang, T. Muhmood, A. Wang, Adsorption and desorption of Pb(II) on l-lysine modified montmorillonite and the simulation of interlayer structure, Appl. Clay Sci. 169 (2019) 40–47, https://doi.org/10.1016/j.clay.2018.12.017.

[26] S.D. Alexandratos, S. Natesan, Ion-selective polymer-supported reagents: the principle of bifunctionality, Eur. Polym. J. 35 (3) (1999) 431–436, https://doi.org/10.1016/S0014-3057(98)00142-6.

[27] S.D. Alexandratos, S.D. Smith, Intraligand cooperation in metal-ion binding by immobilized ligands: the effect of bifunctionality, J. Appl. Polym. Sci. 91 (1) (2004) 463–468, https://doi.org/10.1002/app.13131.

[28] A. Chandrasekar, T.K. Ghanty, C.V.S. Brahmmananda Rao, M. Sundararajan, N. Sivaraman, Strong influence of weak hydrogen bonding on actinide–phosphonate complexation: accurate predictions from DFT followed by experimental validation, Phys. Chem. Chem. Phys. 21 (10) (2019) 5566–5577, https://doi.org/10.1039/C9CP00479C.

[29] D. Gomes Rodrigues, S. Monge, S. Pellet-Rostaing, N. Dacheux, D. Bouyer, C. Faur, Sorption properties of carbamoylmethylphosphonated-based polymer combining both sorption and thermosensitive properties: new valuable hydrosoluble materials for rare earth elements sorption, Chem. Eng. J. 355 (2019) 871–880, https://doi.org/10.1016/j.cej.2018.08.190.

[30] Z. Marczenko, Spectrophotometric determination of elements, Ellis Horwood, Chichester (U.K.),1976.

[31] D.A.A. Thompson, E. Gullikson, M. Howells, K.-J. Kim, J. Kirz, J. Kortright, Y.L.I. Lindau, P. Pianetta, A. Robinson, J. Scofield, J. Underwood, G. Williams, H. Winick, X-ray data booklet, lawrence berkeley national laboratory, university of California, Berkeley, CA, USA2009., (2022).

[32] J. Bai, X. Ma, C. Gong, Y. Chen, H. Yan, K. Wang, J. Wang, A novel amidoxime functionalized porous resins for rapidly selective uranium uptake from solution, J. Mol. Liq. 320 (2020), 114443, https://doi.org/10.1016/j.molliq.2020.114443.

[33] Y. Tian, L. Liu, F. Ma, X. Zhu, H. Dong, C. Zhang, F. Zhao, Synthesis of phosphorylated hyper-cross-linked polymers and their efficient uranium adsorption in water, J. Hazard. Mater. 419 (2021), 126538, https://doi.org/10.1016/j.jhazmat.2021.126538.

[34] K.S.W. Sing, Reporting physisorption data for gas/solid systems with special reference to the determination of surface area and porosity (Recommendations 1984), Pure Appl. Chem. 57 (4) (1985) 603–619, https://doi.org/10.1351/pac198557040603.

[35] C. Salmas, G. Androutsopoulos, Mercury porosimetry: contact angle hysteresis of materials with controlled pore structure, J. Colloid Interface Sci. 239 (2001) 178–189, https://doi.org/10.1006/jcis.2001.7531.

[36] M.C. Zenobi, C.V. Luengo, M.J. Avena, E.H. Rueda, An ATR-FTIR study of different phosphonic acids in aqueous solution, Spectrochim. Acta, Part A 70 (2) (2008) 270–276, https://doi.org/10.1016/j.saa.2007.07.043.

[37] M.C. Zenobi, C.V. Luengo, M.J. Avena, E.H. Rueda, An ATR-FTIR study of different phosphonic acids adsorbed onto boehmite, Spectrochim. Acta, Part A 75 (4) (2010) 1283–1288, https://doi.org/10.1016/j.saa.2009.12.059.

[38] A.M. Borreguero, M.M. Velencoso, J.F. Rodríguez, Á. Serrano, M.J. Carrero, M. J. Ramos, Synthesis of aminophosphonate polyols and polyurethane foams with improved fire retardant properties, Appl. Polym. Sci. 136 (29) (2019) 47780, https://doi.org/10.1002/app.47780.

[39] S.H. Kismat Ara Elachi, M.M. Haque, Ranjan K. Mohapatra, Kudrat-E-Zahan, Synthesis, spectral and thermal characterization of Cu(II) complexes containing schiff base ligands and their antibacterial activity study, Am. J. Mater. Synth. Process 4 (1) (2019) 43–53, https://doi.org/10.11648/j.ajmsp.20190401.16.

[40] M.V. Lopez-Ramon, F. Stoeckli, C. Moreno-Castilla, F. Carrasco-Marin, On the characterization of acidic and basic surface sites on carbons by various techniques, Carbon 37 (8) (1999) 1215–1221, https://doi.org/10.1016/S0008-6223(98)00317-0.

[41] R. Williams, pKa data (compiled by R. Williams), 2022. https://organicchemistrydata.org/hansreich/resources/pka/pka_data/pka-compilation-williams.pdf. (Accessed 9/3/2022 2022).

[42] C. Calvino, M. Piechowicz, S.J. Rowan, S. Schrettl, C. Weder, A versatile colorimetric probe based on thiosemicarbazide–amine proton transfer, Eur. J. Chem. 24 (29) (2018) 7369–7373, https://doi.org/10.1002/chem.201801551.

[43] J.L. Viveros-Ceballos, M. Ordóñez, F.J. Sayago, C. Cativiela, Stereoselective synthesis of α-amino-C-phosphinic acids and derivatives, Molecules (Basel, Switzerland) 21 (9) (2016), https://doi.org/10.3390/molecules21091141.

[44] G. Hägele, Z. Szakács, J. Ollig, S. Hermens, C. Pfaff, NMR-controlled titrations: characterizing aminophosphonates and related structures, Heteroat. Chem. 11 (7) (2000) 562–582, https://doi.org/10.1002/1098-1071(2000)11:7<562::AID-HC16>3.0.CO;2-V.

[45] X. Sun, L. Yang, H. Xing, J. Zhao, X. Li, Y. Huang, H. Liu, Synthesis of polyethylenimine-functionalized poly(glycidyl methacrylate) magnetic microspheres and their excellent Cr(VI) ion removal properties, Chem. Eng. J. 234 (2013) 338–345, https://doi.org/10.1016/j.cej.2013.08.082.

[46] C. Tien. Adsorption Calculations and Modeling, Butterworth-Heinemann, Boston, 1994, https://doi.org/10.1016/B978-0-7506-9121-5.50001-X.

[47] W.H. Cheung, Y.S. Szeto, G. McKay, Intraparticle diffusion processes during acid dye adsorption onto chitosan, Bioresour. Technol. 98 (15) (2007) 2897–2904, https://doi.org/10.1016/j.biortech.2006.09.045.

[48] S.A.M.A. Hubbe, S. Douven, Implications of apparent pseudo-second-order adsorption kinetics onto cellulosic materials: a review, BioRes 14 (3) (2019) 7582–7626.

[49] M.J.A.V. Puccia, On the use of the Dubinin-Radushkevich equation to distinguish between physical and chemical adsorption at the solid-water interface, Colloid Interface Sci. Commun. 41 (2021), 100376.

[50] A. Gladysz-Plaska, M. Majdan, E. Grabias, Adsorption of La, Eu and Lu on raw and modified red clay, J. Radioanal. Nucl. Chem. 301 (1) (2014) 33–40, https://doi.org/10.1007/s10967-014-3111-4.

[51] J. Wang, X. Guo, Adsorption isotherm models: classification, physical meaning, application and solving method, Chemosphere 258 (2020), 127279, https://doi.org/10.1016/j.chemosphere.2020.127279.

[52] C. Duan, Y. Zhang, J. Li, L. Kang, Y. Xie, W. Qiao, C. Zhu, H. Luo, Rapid room-temperature preparation of hierarchically porous metal-organic frameworks for efficient uranium removal from aqueous solutions, Nanomaterials 10 (8) (2020) 1539, https://doi.org/10.3390/nano10081539.

[53] J. Xiao, Y. Jing, X.Q. Wang, Y. Yao, Y.Z. Jia, Preconcentration of uranium(VI) from aqueous solution by amidoxime-functionalized microspheres silica material: Kinetics, isotherm and mechanism study, Chemistryselect 3 (43) (2018) 12346–12356, https://doi.org/10.1002/slct.201802472.

[54] S. Liu, J. Luo, J. Ma, J. Li, S. Li, L. Meng, S. Liu, Removal of uranium from aqueous solutions using amine-functionalized magnetic platelet large-pore SBA-15, J. Nucl. Sci. Technol. 58 (1) (2020) 29–39, https://doi.org/10.1080/00223131.2020.1796838.

[55] Y. Wang, X. Hu, Y. Liu, Y. Li, T. Lan, C. Wang, Y. Liu, D. Yuan, X. Cao, H. He, L. Zhou, Z. Liu, J.W. Chew, Assembly of three-dimensional ultralight poly (amidoxime)/graphene oxide nanoribbons aerogel for efficient removal of uranium (VI) from water samples, Sci. Total. Environ. 765 (2021), 142686, https://doi.org/10.1016/j.scitotenv.2020.142686.

[56] J. Zhu, Q. Liu, J. Liu, R. Chen, H. Zhang, R. Li, J. Wang, Ni–Mn LDH-decorated 3D Fe-inserted and N-doped carbon framework composites for efficient uranium(vi) removal, Environ. Sci.: Nano 5 (2) (2018) 467–475, https://doi.org/10.1039/C7EN01018D.

[57] D.A. Giannakoudakis, I. Anastopoulos, M. Barczak, E. Alphantoniou, K. Terpilowski, E. Mohammadi, M. Shams, E. Coy, A. Bakandritsos, I. A. Katsoyiannis, J.C. Colmenares, I. Pashalidis, Enhanced uranium removal from acidic wastewater by phosphonate-functionalized ordered mesoporous silica: surface chemistry matters the most, J. Hazard. Mater. 413 (2021), 125279, https://doi.org/10.1016/j.jhazmat.2021.125279.

[58] R. Karan, K.C. Rajan, T. Sreenivas, Studies on lowering of uranium from mine water by static bed ion exchange process, Sep. Sci. Technol. 54 (10) (2019) 1607–1619, https://doi.org/10.1080/01496395.2019.1572188.

[59] Y. Liu, C. Chen, L. He, L. Hu, Z. Ding, S. Liao, N. Tan, Preparation of a fungal-modified material linked by the monoamidoxime terminal open-chain polyether and its uranyl adsorption, Ind. Eng. Chem. Res. 60 (12) (2021) 4705–4713, https://doi.org/10.1021/acs.iecr.0c05213.

[60] M. Zhang, M. Yuan, M. Zhang, M. Wang, J. Chen, R. Li, L. Qiu, X. Feng, J. Hu, G. Wu, Efficient removal of uranium from diluted aqueous solution with hydroxypyridone functionalized polyethylene nonwoven fabrics, Radiat. Phys. Chem. 171 (2020), 108742, https://doi.org/10.1016/j.radphyschem.2020.108742.

[61] J. Han, L. Hu, L. He, K. Ji, Y. Liu, C. Chen, X. Luo, N. Tan, Preparation and uranium (VI) biosorption for tri-amidoxime modified marine fungus material, Environ. Sci. Pollut. Res. Int. 27 (30) (2020) 37313–37323, https://doi.org/10.1007/s11356-020-07746-z.

[62] P. Hermann, I. Lukeš, Complexing properties of phosphonodipeptides containing aminomethylphosphonic acid, J. Chem. Soc., Dalton Trans. 16 (1995) 2605–2610, https://doi.org/10.1039/DT9950002605.